Editors' Suggestion

Dynamical Scaling and Planckian Dissipation Due to Heavy-Fermion Quantum Criticality

Andreas Gleis,[1,2,*] Seung-Sup B. Lee,[3,4,5,1,†] Gabriel Kotliar,[2,6,‡] and Jan von Delft[1,§]

[1]*Arnold Sommerfeld Center for Theoretical Physics, Center for NanoScience, and Munich Center for Quantum Science and Technology, Ludwig-Maximilians-Universität München, 80333 Munich, Germany*
[2]*Department of Physics and Astronomy, Rutgers University, Piscataway, New Jersey 08854, USA*
[3]*Department of Physics and Astronomy, Seoul National University, Seoul 08826, Korea*
[4]*Center for Theoretical Physics, Seoul National University, Seoul 08826, Korea*
[5]*Institute for Data Innovation in Science, Seoul National University, Seoul 08826, Korea*
[6]*Condensed Matter Physics and Materials Science Department, Brookhaven National Laboratory, Upton, New York 11973, USA*

(Received 24 June 2024; accepted 23 January 2025; published 10 March 2025)

We study dynamical scaling associated with a Kondo-breakdown quantum-critical point (KB QCP) of the periodic Anderson model, treated by two-site cellular dynamical mean-field theory (2CDMFT). In the quantum-critical region, the dynamical staggered-spin susceptibility exhibits ω/T scaling. We propose a scaling ansatz that describes this behavior and reveals Planckian dissipation for the longest-lived excitations. The current susceptibility follows the same scaling, leading to strange-metal behavior for the optical conductivity and resistivity. Importantly, this behavior is driven by strong short-ranged vertex contributions, not single-particle decay. This suggests that the KB QCP described by 2CDMFT is a novel *intrinsic* (i.e., disorder-free) strange-metal fixed point. Our results for the optical conductivity match experimental observations on $YbRh_2Si_2$ and $CeCoIn_5$.

DOI: 10.1103/PhysRevLett.134.106501

Introduction—Strange metals [1–5], an enigmatic state of matter found in many strongly correlated materials [6–27], still defy a clear and unified understanding. Their phenomenology, including a low-temperature ($\gtrsim$10 mK in $YbRh_2Si_2$ [28]) T-linear resistivity [9], an $\sim T \ln T$ specific heat and ω/T scaling [8,24,26,29–32], is incompatible with normal Fermi liquids [33]. Despite the ubiquity of strange metals, many basic questions remain unsettled [1], in particular, whether intrinsic strange metals, i.e., ones without disorder, exist [34,35].

Current attempts at explaining strange-metal phenomena often employ the marginal Fermi liquid (MFL) hypothesis [36], where electrons acquire a linear-in-T scattering rate due to scattering by a critical bosonic mode. However, it has recently been shown within the Yukawa-Sachdev-Ye-Kitaev (YSYK) approach that interaction disorder is required to also achieve a linear-in-T transport scattering rate [37,38]; i.e., the MFL strange metal is not intrinsic. The same goes for MFL strange metals arising in single-site dynamical mean-field theory (DMFT) approaches [39], where single-electron and transport scattering rates coincide due to nonconserved momentum at the interaction vertex [40,41]. It is questionable whether the MFL approach can be reconciled with studies of disorder in cuprates [42], the fact that many strange metals are very clean [28,43] and with Hall angle measurements in strange metals [1,16,44–50].

In this Letter, we present a novel approach to intrinsic strange metals where phenomena like ω/T scaling and a linear-in-T resistivity arise from collective short-ranged fluctuations. The single-electron scattering rate does not play a direct role, in stark contrast to MFL approaches. We focus on heavy-fermion (HF) metals, where strange-metal behavior routinely emerges in the quantum-critical region of so-called Kondo breakdown (KB) quantum-critical points (QCPs) [51–56]. Previous studies have obtained interesting scaling behavior in the vicinity of a KB QCP [38,51,57–60], but apart from the MFL-based YSYK approach of Ref. [38], none of these studies explain the intriguing optical properties of HF strange metals.

We study the quantum-critical region of a KB QCP in the periodic Anderson model (PAM) described as a continuous orbital-selective Mott transition [56,61–64] via two-site cellular DMFT (2CDMFT) [41,65]. 2CDMFT maps the PAM to a self-consistent two-impurity Anderson model [56,61–64]. In a long companion paper [56], we

*Contact author: andreas.gleis@rutgers.edu
†Contact author: sslee@snu.ac.kr
‡Contact author: kotliar@physics.rutgers.edu
§Contact author: vondelft@lmu.de

used the numerical renormalization group (NRG) [66–71] as an impurity solver for 2CDMFT to identify a novel, 2CDMFT-stabilized KB QCP (by contrast, the Jones–Varma QCP is unstable [72–88]). We find ω/T scaling for several susceptibilities and strange-metal behavior for the optical conductivity and resistivity. Importantly, this behavior arises from dominant vertex contributions rather than single-particle decay.

Model and methods—We consider the PAM on a three-dimensional cubic lattice, involving an itinerant c band and a localized f band described by the Hamiltonian

$$H_{\mathrm{PAM}} = \sum_{\mathbf{k}\sigma}(\epsilon_f - \mu) f^\dagger_{\mathbf{k}\sigma} f_{\mathbf{k}\sigma} + U \sum_i f^\dagger_{i\uparrow} f_{i\uparrow} f^\dagger_{i\downarrow} f_{i\downarrow} + V \sum_{\mathbf{k}\sigma}(c^\dagger_{\mathbf{k}\sigma} f_{\mathbf{k}\sigma} + \mathrm{H.c.}) + \sum_{\mathbf{k}\sigma}(\epsilon_{c\mathbf{k}} - \mu) c^\dagger_{\mathbf{k}\sigma} c_{\mathbf{k}\sigma}. \tag{1}$$

Here, $f^\dagger_{\mathbf{k}\sigma}[c^\dagger_{\mathbf{k}\sigma}]$ creates a spin-$\sigma f[c]$ electron with momentum $\mathbf{k}$, and $\epsilon_{c\mathbf{k}} = -2t\sum_{a=x,y,z}\cos(k_a)$ is the c-electron dispersion. We set the c-electron hopping $t = 1/6$ as an energy unit (half bandwidth $= 1$) and fix the f-orbital level $\epsilon_f = -5.5$, the interaction strength $U = 10$, and the chemical potential $\mu = 0.2$, as chosen in prior 2CDMFT studies [56,63,64]. The (T, V) phase diagram studied in detail in Ref. [56] (shown also in Ref. [89], Sec. S-I) is characterized by two V-dependent energy scales T_{FL} and T_{NFL}: The FL scale T_{FL}, below which FL behavior emerges, decreases toward and vanishes at the KB QCP at $V_c = 0.4575(25)$. This gives rise to a quantum-critical region between the scales $T_{\mathrm{FL}} < T_{\mathrm{NFL}}$, where we found non-Fermi liquid (NFL) behavior with strange-metal properties, such as a $T\ln T$ specific heat [56].

In this work, we study dynamical scaling and optical properties in the quantum-critical region. We fix $V = 0.46 \gtrsim V_c$ [96] and tune T. At $V = 0.46$, $T_{\mathrm{NFL}}/T_{\mathrm{FL}} > 10^3$; i.e., the NFL region extends over more than three decades, which allows us to study scaling. As in Ref. [56], we enforce U(1) charge and SU(2) spin symmetries (using the QSpace tensor library [97–99]), thereby excluding the possibility of symmetry breaking order by hand. We do not find tendencies toward symmetry breaking (divergent susceptibilities) for the parameters studied here.

Dynamical scaling—As a result of incomplete screening in the NFL region, many dynamical susceptibilities

$$\chi[\mathcal{A},\mathcal{B}](\omega) = -\mathrm{i}\int_0^\infty \mathrm{d}t\, \mathrm{e}^{\mathrm{i}(\omega+\mathrm{i}0^+)t}\langle[\mathcal{A}(t),\mathcal{B}^\dagger]\rangle \tag{2}$$

exhibit plateaus in their spectra $\chi''(\omega)$ at $T_{\mathrm{FL}} < \omega < T_{\mathrm{NFL}}$ and $T = 0$; cf. Ref. [56], Fig. 4. We use the shorthand $\chi[\mathcal{A}](\omega) = \chi[\mathcal{A},\mathcal{A}](\omega)$ and $\chi(\omega) = \chi'(\omega) - \mathrm{i}\pi\chi''(\omega)$. An example of a susceptibility governed by incomplete screening is $\chi[X^{xz}](\omega, T)$, where $X^{xz} = S^z_1 - S^z_2$ is the staggered f-electron spin on a two-site cluster. It exhibits ω/T scaling, as demonstrated in Fig. 1.

The T-dependent spectra $\chi''(\omega, T)$ and the corresponding real parts $\chi'(\omega, T)$ are shown in Figs. 1(a) and 1(b), respectively. As T is decreased from around T_{NFL} to T_{FL}, the aforementioned plateau in $\chi''(\omega, T)$ emerges between $T < \omega < T_{\mathrm{NFL}}$, crossing over to $\propto \omega$ behavior for $\omega < T$. For $T < T_{\mathrm{FL}}$, the spectrum becomes T independent. In the (imaginary) time domain, the plateau in χ'' implies SYK-like slow $1/\tau$ dynamics; see Fig. S1 of Ref. [89].

$\chi'(\omega, T)$ is related to $\chi''(\omega, T)$ via a Kramers-Kronig relation. It thus shows a logarithmic [100] ω dependence for $\max(T, T_{\mathrm{FL}}) < \omega < T_{\mathrm{NFL}}$ and is constant for $\omega < \max(T, T_{\mathrm{FL}})$. As a result, $\chi'(0, T)$ [inset of Fig. 1] has a $\propto \ln T$ dependence for $T_{\mathrm{FL}} < T < T_{\mathrm{NFL}}$ and is constant for $T < T_{\mathrm{FL}}$, where X^{xz} fluctuations are screened.

Figure 1(c) shows $\chi''(\omega, T)$ vs ω/T. In the NFL region ($T_{\mathrm{FL}} < T < T_{\mathrm{NFL}}$, $|\omega| < T_{\mathrm{NFL}}$), the spectra all collapse onto a single curve. This demonstrates dynamical scaling in the sense that $T^\alpha\chi''(\omega, T) = \mathcal{X}''(\omega/T)$ with $\alpha = 0$. The real part [Fig. 1(d)] also shows ω/T scaling.

Scaling function and Planckian dissipation—In the NFL region ($T_{\mathrm{FL}} < T < T_{\mathrm{NFL}}$, $|\omega| < T_{\mathrm{NFL}}$), the spectra of dynamical susceptibilities showing plateaus (e.g., $\chi[X^{xz}]$) can be fitted with a phenomenological ansatz for $\omega > 0$:

$$\tilde{\chi}''(\omega, T) = \chi_0 \int_T^{T_{\mathrm{NFL}}} \frac{\mathrm{d}\epsilon}{\pi} \frac{\left(1 - \mathrm{e}^{-\frac{\omega}{T}}\right)\left(\frac{\epsilon}{T}\right)^\nu bT}{(\omega - a\epsilon)^2 + (bT)^2}. \tag{3}$$

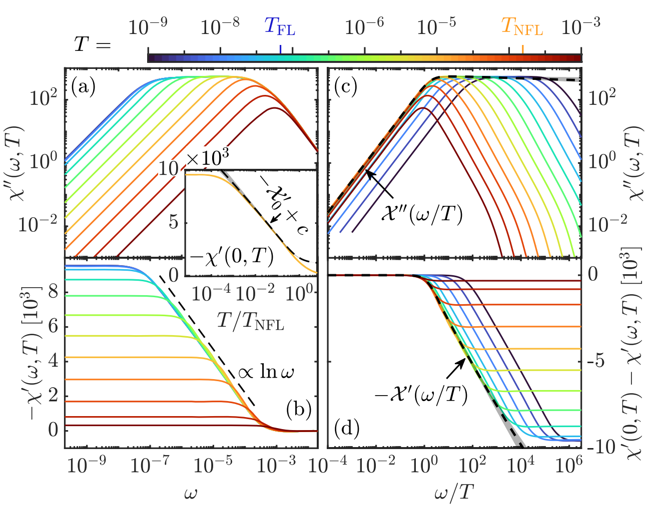

FIG. 1. Dynamical susceptibility $\chi[X^{xz}](\omega, T)$. (a) Spectral part and (b) corresponding real part for 13 choices of T (marked by ticks on the color bar). (c),(d) Scaling collapse of spectral and real parts. Black dashed lines show the universal scaling functions $\mathcal{X}''(\omega/T)$ and $\mathcal{X}'(\omega/T)$, respectively [cf. Eq. (4)]. Inset: $\chi'(0, T)$ (orange) and $\mathcal{X}'_0(T/T_{\mathrm{NFL}}) + c$ [black dashed; cf. Eq. (4)]. The constant shift c accounts for spectral weight at $|\omega| > T_{\mathrm{NFL}}$. Gray areas indicate fitting uncertainties [89].

$\omega < 0$ follows from antisymmetry of $\tilde{\chi}''$, and the real part $\tilde{\chi}'$ is determined through a Kramers-Kronig relation. χ_0, a, b, and ν are determined by fits to our spectra in the NFL region [89]. We find $a \simeq 10^{-1}$, $b \simeq 1$, and $\nu \simeq 0$; χ_0 determines the plateau value. (These parameters are V independent within our fitting accuracy.) When Eq. (3) is evaluated for $|\omega|, T \ll T_{\mathrm{NFL}}$ one finds the scaling form

$$\tilde{\chi}(\omega, T) \simeq \mathcal{X}_0'\left(\frac{T}{T_{\mathrm{NFL}}}\right) + \mathcal{X}'\left(\frac{\omega}{T}\right) - \mathrm{i}\pi\mathcal{X}''\left(\frac{\omega}{T}\right). \quad (4)$$

An explicit T dependence, due to the high-energy cutoff T_{NFL}, only enters via $\mathcal{X}_0'(T/T_{\mathrm{NFL}}) \simeq \tilde{\chi}'(0, T)$; otherwise, $\tilde{\chi}(\omega, T)$ only depends on the ratio ω/T (for more information on the universal scaling functions $\mathcal{X}_0'$, $\mathcal{X}'$, and $\mathcal{X}''$, see Ref. [89]). In Figs. 1(c) and 1(d), we show that the scaling function $\mathcal{X}$ captures $\chi[X^{xz}]$ well in the NFL region (black dashed lines).

The ansatz (3) is motivated by a fit of $\langle X^{xz}(t) X^{xz}\rangle$ to a superposition of coherent excitations with mean energy $a\epsilon$, decay rate bT, and density of states $(\epsilon/T)^\nu$ [89]. Since $b \simeq 1$, these coherent excitations have a decay rate $\gamma \simeq T$ or correspondingly a lifetime $\tau \simeq 1/T$; i.e., the longest-lived X^{xz} excitations have a Planckian lifetime.

Optical conductivity—Our 2CDMFT approximation allows us to compute the *local* current susceptibility $\chi[j_i^a](\omega, T)$ of the lattice model from the effective impurity model. Here, $j_i^a = -\mathrm{i}te \sum_\sigma (c_{i\sigma}^\dagger c_{i+\mathbf{a}\sigma} - c_{i+\mathbf{a},\sigma}^\dagger c_{i\sigma})$ is the current operator in the a direction, with i and $i + \mathbf{a}$ nearest neighbors on the lattice, chosen to also correspond to the two sites of the self-consistent impurity model.

For optical experiments and electronic transport, the uniform current susceptibility $\chi[j_{\mathbf{q}=\mathbf{0}}^a](\omega, T)$ is relevant, where $j_{\mathbf{q}}^a$ is the $\mathbf{q}$-dependent current in the a direction $j_{\mathbf{q}}^a = (1/N)\sum_{i\sigma} \mathrm{e}^{-\mathrm{i}\mathbf{q}\cdot\mathbf{r}_i} j_i^a$. Assuming translation symmetry, $\chi[j_{\mathbf{0}}^a]$ can be expressed as a sum $\chi[j_i^a] + \chi_{\mathrm{nl}}[j]$ of local and nonlocal parts, with $\chi_{\mathrm{nl}}[j] = (1/N)\sum_{\ell \neq i} \chi[j_\ell^a, j_i^a] = \chi[j_{\mathbf{0}}^a] - \chi[j_i^a]$. The computation of $\chi_{\mathrm{nl}}[j]$ would require four-point correlators [101–103] for the self-consistent two-impurity model, which currently exceeds our computational resources. Hence, we approximate it by its bubble contribution $\chi_{\mathrm{nl,B}}[j] = \chi_{\mathrm{B}}[j_{\mathbf{0}}^a] - \chi_{\mathrm{B}}[j_i^a]$. Thus, we use

$$\chi[j_{\mathbf{0}}^a] \approx \chi[j_i^a] + \chi_{\mathrm{nl,B}}[j] = \chi_{\mathrm{B}}[j_{\mathbf{0}}^a] + \chi_{\mathrm{vtx}}[j_i^a], \quad (5)$$

where $\chi_{\mathrm{vtx}}[j_i^a] = \chi[j_i^a] - \chi_{\mathrm{B}}[j_i^a]$ is the *vertex* contribution to the local current susceptibility.

The uniform current spectrum determines the real part of the optical conductivity $\sigma'(\omega, T) = (\pi/\omega)\chi''[j_{\mathbf{0}}^a](\omega, T)$ shown in Fig. 2(a). At $T \ll T_{\mathrm{FL}}$ (blue and black), it features a hybridization gap around $\omega \simeq T_{\mathrm{NFL}}$, ω^{-1} behavior for $T_{\mathrm{FL}} < \omega < T_{\mathrm{NFL}}$, and a Drude peak at low frequencies below T_{FL}. These features emerge as the temperature is lowered from $T \gg T_{\mathrm{NFL}}$: The hybridization gap forms around $T \simeq T_{\mathrm{NFL}}$ (red), the ω^{-1} feature emerges between $T_{\mathrm{FL}} < T < T_{\mathrm{NFL}}$ (yellow and green), and the Drude peak finally emerges for $T < T_{\mathrm{FL}}$ (blue and black).

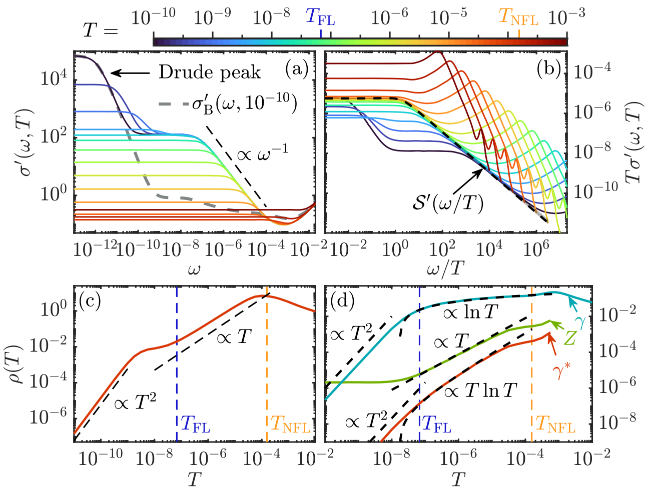

FIG. 2. (a) Real part of the optical conductivity $\sigma'(\omega, T)$; gray dashed line, bubble contribution at $T = 10^{-10}$. (b) ω/T scaling of $T\sigma'(\omega, T)$; black dashed line, the scaling function $\mathcal{S}'$ of Eq. (6). (c) The resistivity $\rho(T)$. (d) The single-particle decay rate γ, quasiparticle (QP) weight Z, and QP decay rate γ^*.

The ω^{-1} feature in the NFL region is due to ω/T scaling of $\chi''[j_i^a]$ (Fig. S5 in Ref. [89]) similar to that of $\chi''[X^{xz}]$. Remarkably, $\chi''[j_i^a]$, just as $\chi''[X^{xz}]$, is well described by the ansatz (3) (see Fig. S8 of Ref. [89]), implying ω/T scaling and Planckian dissipation of current fluctuations. In the NFL region, $T_{\mathrm{FL}} < T < T_{\mathrm{NFL}}$, $\sigma'(\omega, T)$ is therefore governed by a scaling function $\mathcal{S}'$:

$$T\sigma'(\omega, T) = (T/\omega)\pi\mathcal{X}''(\omega/T) = \mathcal{S}'(\omega/T). \quad (6)$$

Figure 2(b) shows that $T\sigma'(\omega, T)$ is indeed well described by this scaling function (black dashed line). Similarly, we find that $T\sigma''(\omega, T) = \mathcal{S}''(\omega/T)$, with $\mathcal{S}''(x) = \mathcal{X}'(x)/x$; see Ref. [89], Secs. S–V, Fig. S10.

The scaling behavior (6) has two striking implications for the NFL region $T_{\mathrm{FL}} < T < T_{\mathrm{NFL}}$: First, a scaling collapse is achieved for $T^\alpha \sigma'(\omega, T)$ with $\alpha = 1$, an exponent which was also found experimentally [24,26,32]. Second, the static conductivity $\sigma(T) = \sigma'(0, T) = \mathcal{S}'(0)/T$ scales as $1/T$, implying T-linear behavior for the resistivity, $\rho(T) = 1/\sigma(T) \propto T$. This is borne out in Fig. 2(c): $\rho(T)$ has a maximum around T_{NFL}, where the hybridization gap forms, then decreases $\propto T$ for $T_{\mathrm{FL}} < T < T_{\mathrm{NFL}}$, before finally becoming $\propto T^2$ below T_{FL}.

The ω/T scaling and linear-in-T resistivity in the NFL region is completely dominated by the vertex contribution to the current susceptibility $\chi''_{\mathrm{vtx}}[j_i^a]| \gg |\chi''_{\mathrm{B}}[j_{\mathbf{0}}^a]|$. To visualize this, we have included the bubble contribution $\sigma'_{\mathrm{B}}(\omega)$ (gray dashed) at $T = 10^{-10}$ in Fig. 2(a). In the NFL region ($T_{\mathrm{FL}} < |\omega| < T_{\mathrm{NFL}}$), σ'_{B} is orders of magnitude smaller than $\sigma'(\omega)$ and, crucially, does not show ω^{-1} behavior. Also, $\sigma'_{\mathrm{B}}(\omega, T)$ does not exhibit ω/T scaling. However, it contributes the Drude peak at $|\omega|, T < T_{\mathrm{FL}}$.

Next, we consider the single-particle decay rate γ [104], QP weight Z, and QP decay rate γ^*,

$$\gamma = \mathrm{Im} G^{-1}_{\mathbf{k}_{\mathrm{F}}}(0), \quad Z^{-1} = \partial_\omega \mathrm{Re} G^{-1}_{\mathbf{k}_{\mathrm{F}}}(0), \quad \gamma^* = Z\gamma \tag{7}$$

shown in Fig. 2(d). Z and γ^* determine the weight and width of the Lorenzian line shape in the single-particle spectral function at $\mathbf{k}_{\mathrm{F}}$, while γ governs the bubble contribution to the conductivity $\sigma'_{\mathrm{B}} \propto 1/\gamma$. In the NFL region, we find $\gamma \propto \ln T$, i.e., $\sigma'_{\mathrm{B}} \propto 1/\ln T \ll \sigma' \propto 1/T$. Thus, the conductivity in the NFL region is not governed by single-particle decay but by short-ranged collective current fluctuations, in contrast to the MFL paradigm.

In the FL region, $\gamma, \gamma^* \propto T^2$, and $Z = \mathrm{const}$ [Fig. 2(d)] as expected, leading to a Drude peak of width $\propto T^2$ and $\rho(T) \propto T^2$; i.e., these features are due to long-lived coherent QP carrying the current. Since we neglect *non-local* vertex contributions which encode momentum conservation during small-momentum scattering [105], the transport relaxation rate, and thus the T^2 prefactor of $\rho(T)$, is set purely by the QP decay rate and is therefore very likely overestimated.

Optical mass and transport scattering rate—To obtain additional insights, we determined the transport scattering rate $\tau^{-1}(\omega)$ and the optical mass $m^*(\omega)$ defined as

$$\tau^{-1}(\omega) = \mathrm{Re}\sigma^{-1}(\omega), \qquad m^*(\omega) = -\omega^{-1}\mathrm{Im}\sigma^{-1}(\omega) \tag{8}$$

following Ref. [106], Eq. (1). Here, $\sigma(\omega)$ is the complex optical conductivity, and we omitted constant prefactors to focus on qualitative features.

Figure 3(a) shows our results for $\tau^{-1}(\omega)$, with $\tau^{-1}(0) = \tau_0^{-1} = \rho(T) \propto T$ for $T_{\mathrm{FL}} < T < T_{\mathrm{NFL}}$. For $\max(T_{\mathrm{FL}}, T) < |\omega| < T_{\mathrm{NFL}}$, $\tau^{-1}(\omega)$ has a nontrivial ω and T dependence, not following a simple power law with possible logarithmic corrections. There, $\sigma(\omega)$ does not fit a Drude form. Non-Drude behavior is most clearly visible from $\sigma'(\omega, T)$ [cf. Fig. 2(a)], which shows a ω^{-1} dependence in the NFL region, whereas a usual Drude peak would imply an ω^{-2} dependence. Similar non-Drude behavior of the optical conductivity has been observed in $\mathrm{YbRh_2Si_2}$ [24,26].

Remarkably, in the NFL region ($T_{\mathrm{FL}} < T < T_{\mathrm{NFL}}$) at low frequencies $|\omega| \lesssim T$, $\tau^{-1}(\omega)$ shows a quadratic frequency dependence $\tau^{-1}(\omega) - \tau_0^{-1} \sim c(T)\omega^2$; cf. Fig. 3(c). An ω^2 dependence of $\tau^{-1}(\omega)$ was also found in $\mathrm{CeCoIn_5}$; cf. Figs. 4(a) and 4(c) of Ref. [106] and its discussion. However, whereas for an FL the prefactor $c(T)$ does not depend on the temperature, the ω/T scaling of $\sigma(\omega, T)$ in the strange-metal region implies $c(T) \sim 1/T$; see Ref. [89], Sec. S–V.

We emphasize that in our results, $\tau^{-1}(\omega)$ is not proportional to $-\mathrm{Im}\Sigma(\omega)$ (without vertex contributions, a

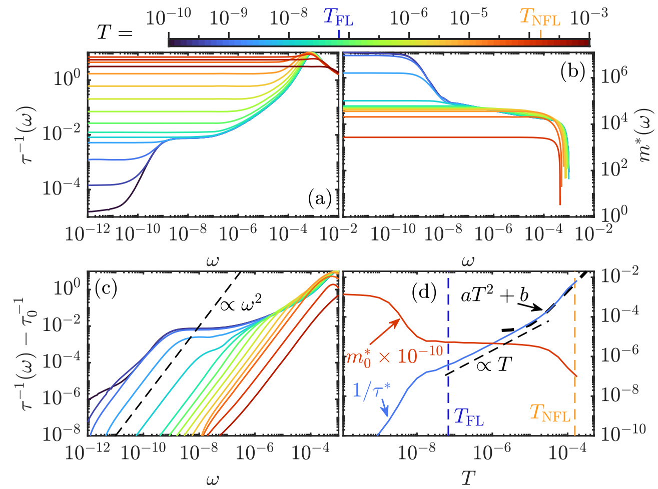

FIG. 3. Frequency dependence of (a) the transport scattering rate $\tau^{-1}(\omega)$, (b) the effective mass $m^*(\omega)$, and (c) $\tau^{-1}(\omega) - \tau_0^{-1}$, where $\tau_0^{-1} = \tau^{-1}(0) = \rho$. (d) Temperature dependence of $\tau^{*-1} = \tau_0^{-1}/m_0^*$ and $m_0^* = m^*(0)$.

proportionality would be expected). In our 2CDMFT + NRG approach to the PAM, $-\mathrm{Im}\Sigma(\omega)$ has a logarithmic ω and T dependence; cf. Figs. 11 and 12 of Ref. [56]. The ω and T dependence $\tau^{-1}(\omega)$ discussed above differs from that, again illustrating the importance of vertex contributions.

Figure 3(b) shows $m^*(\omega)$. In the NFL region ($T_{\mathrm{FL}} < T < T_{\mathrm{NFL}}$), $m^*(\omega)$ is strongly frequency dependent around the NFL scale $\omega \simeq 10^{-3} - 10^{-4} \simeq T_{\mathrm{NFL}}$, and then saturates to an almost ω- and T-independent value $m^*(\omega) \simeq m^*(0) = m_0^*$. The weak ω and T dependence of $m^*(\omega)$ does not seem to follow a simple power law. Interestingly, even though there are no well-defined QPs in the strange-metal region, there nevertheless seems to be a somewhat well-defined effective mass m_0^*. We emphasize though that in the NFL region, $m_0^* \simeq 5 \times 10^4 \sim 10/T_{\mathrm{NFL}}$ is orders of magnitude smaller than in the FL region, where $m_0^* \simeq 1.5 \times 10^7 \sim 1/T_{\mathrm{FL}}$; cf. Fig. 3(d). The effective mass in the NFL region is therefore decisively distinct from the QP mass in the low-temperature FL region.

In Fig. 3(d), we show the temperature dependence of the renormalized scattering rate $\tau^{*-1} = \tau_0^{-1}/m_0^*$ (blue), together with m_0^* (red). Deep in the NFL region, we find $\tau^{*-1} \sim T$, since $\tau_0^{-1} \sim T$ and $m_0^* = \mathrm{const}$. Interestingly, in the crossover region between $T \simeq T_{\mathrm{NFL}}$ and $T \simeq 10^{-1}T_{\mathrm{NFL}}$, τ^{*-1} deviates from the linear-in-T behavior and is consistent with FL-like T^2 behavior.

A similar T^2 behavior was reported for $\mathrm{CeCoIn_5}$ in Ref. [106], where this behavior was interpreted as evidence for a hidden Fermi liquid. Our calculations suggest that the T^2 behavior is rather a crossover behavior, and measurements at lower temperatures are necessary for a definite conclusion. Such measurements are presumably not possible in $\mathrm{CeCoIn_5}$ due to its relatively high T_c. A promising candidate material to clarify whether $\tau^{*-1} \sim T$ or $\sim T^2$ may

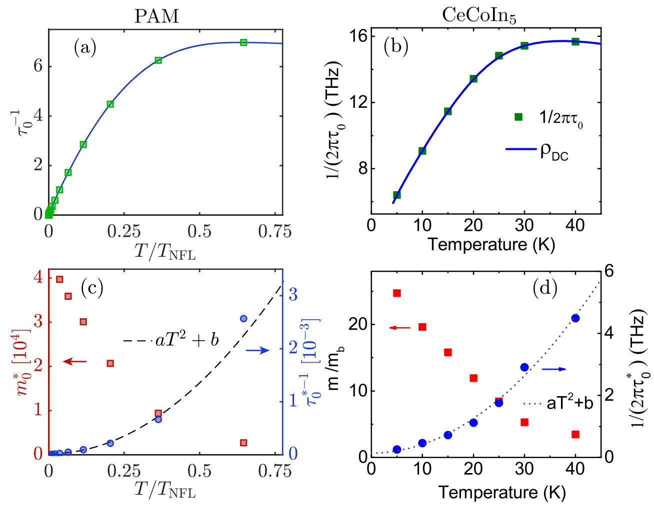

FIG. 4. (a) Scattering rate $\tau_0^{-1} = \rho(T)$ for $T \lesssim T_{\rm NFL}$ for the PAM. Green squares, data points; blue line, guide to the eye. (b) τ_0^{-1} (green squares) and rescaled resistivity (blue line) for $CeCoIn_5$ close to its coherence temperature $T^* = 40$ K, adapted from Fig. 4(b) of Ref. [106]. (c) Renormalized scattering rate τ_0^{*-1} (blue circles) and effective mass m_0^* (red squares) for the PAM. (d) τ_0^{*-1} (blue circles) and m_0^* (red squares) for $CeCoIn_5$, adapted from Fig. 4(d) of Ref. [106].

be $YbRh_2Si_2$. To emphasize the similarity between the experimental data on $CeCoIn_5$ and our results on the PAM more visually, we show the resistivity $\rho(T)$ of the PAM in Fig. 4(a) on a linear scale in the crossover region, next to the corresponding experimental data on $CeCoIn_5$ [Fig. 4(b)], adapted from Fig. 4(b) of Ref. [106]. In Figs. 4(c) and 4(d), we further show the data for the renormalized scattering rate and the effective mass for both the PAM and $CeCoIn_5$, respectively [adapted from Fig. 4(d) of Ref. [106] for the latter]. The experimental data on $CeCoIn_5$ and our numerical data on the PAM show remarkable qualitative agreement in the crossover region: (i) The resistivity has a broad maximum and turns to linear in T, (ii) the renormalized scattering rate $\tau^{*-1} \propto T^2$, and (iii) the effective mass m_0^* increases with the temperature in a remarkably similar fashion. An estimate of the suitability of our model parameters for $CeCoIn_5$ is provided in Ref. [89]. A more detailed quantitative description of $CeCoIn_5$ (or $YbRh_2Si_2$) will require a more realistic future study, e.g., using LDA + DMFT + NRG.

Discussion and outlook—Our work provides a promising route toward an intrinsic strange metal. However, we have not yet achieved a full understanding of the current decay mechanism. An inherent feature of (C)DMFT is that the interaction vertex does not ensure conservation of crystal momentum [40,41]. Therefore, electron-electron scattering does not conserve crystal momentum, leading to current decay. This mechanism usually manifests as a dominant bubble contribution (in single-site DMFT, this is the only contribution). A dominant bubble contribution is also key to the YSYK approach [37] to strange metals. There, a disordered Yukawa coupling leads to nonconserved momentum in scattering processes. The result is an MFL where strange-metal scaling arises in the bubble contribution, and interaction disorder is needed to avoid its cancellation by the vertex contribution. By contrast, in our 2CDMFT approach, the strange-metal scaling in the NFL region arises *entirely from the vertex contribution*, and not at all from the (much smaller) bubble contribution. This strongly suggests that the current decay mechanism is not due to the nonconservation of crystal momentum at the interaction vertex. Our 2CDMFT approach also includes crystal momentum conserving umklapp scattering processes between momenta around $\mathbf{k} = (0,0,0)$ and $\mathbf{k} = (\pi,\pi,\pi)$ which flip the current. We conjecture that these cause our observed strange-metal scaling, but leave a detailed analysis for future work.

Acknowledgments—We thank Assa Auerbach, Silke Bühler-Paschen, Andrey Chubukov, Piers Coleman, Dominic Else, Fabian Kugler, Antoine Georges, Sean Hartnoll, Andy Millis, Achim Rosch, Subir Sachdev, Qimiao Si, Katharina Stadler, Senthil Todadri, Matthias Vojta, Andreas Weichselbaum, and Krzysztof Wójcik for helpful discussions. This work was funded in part by the Deutsche Forschungsgemeinschaft under Germany's Excellence Strategy EXC-2111 (Project No. 390814868). It is part of the Munich Quantum Valley supported by the Bavarian state government with funds from the Hightech Agenda Bayern Plus. This work was further supported by Grants No. INST 86/1885-1 FUGG and No. LE 3883/2-2 of the German Research Foundation. S. S. B. L. was supported by Samsung Electronics Co., Ltd. (Grant No. IO220817-02066-01), the Global-LAMP Program of the National Research Foundation of Korea (NRF) grant funded by the Ministry of Education (Grant No. RS-2023-00301976), the NRF grant funded by the Korean government (MSIT) (Grant No. RS-2023-00214464), and the NRF grant funded by the Korean government (MEST) (Grant No. 2019R1A6A1A10073437). The National Science Foundation supported G. K. under Grant No. DMR-1733071, and J. v. D. in part under Grant No. PHY-1748958. A. G. acknowledges support from the Abrahams Postdoctoral Fellowship of the Center for Materials Theory at Rutgers University.

[1] P. W. Phillips, N. E. Hussey, and P. Abbamonte, Stranger than metals, Science **377**, eabh4273 (2022).
[2] S. A. Hartnoll and A. P. Mackenzie, Colloquium: Planckian dissipation in metals, Rev. Mod. Phys. **94**, 041002 (2022).
[3] D. Chowdhury, A. Georges, O. Parcollet, and S. Sachdev, Sachdev-Ye-Kitaev models and beyond: Window into non-Fermi liquids, Rev. Mod. Phys. **94**, 035004 (2022).

[4] J. Zaanen, Why the temperature is high, Nature (London) **430**, 512 (2004).

[5] J. G. Checkelsky, B. A. Bernevig, P. Coleman, Q. Si, and S. Paschen, Flat bands, strange metals and the Kondo effect, Nat. Rev. Mater. **9**, 509 (2024).

[6] B. Keimer, S. A. Kivelson, M. R. Norman, S. Uchida, and J. Zaanen, From quantum matter to high-temperature superconductivity in copper oxides, Nature (London) **518**, 179 (2015).

[7] B. Michon, C. Girod, S. Badoux, J. Kačmarčík, Q. Ma, M. Dragomir, H. A. Dabkowska, B. D. Gaulin, J.-S. Zhou, S. Pyon, T. Takayama, H. Takagi, S. Verret, N. Doiron-Leyraud, C. Marcenat, L. Taillefer, and T. Klein, Thermodynamic signatures of quantum criticality in cuprate superconductors, Nature (London) **567**, 218 (2019).

[8] B. Michon, C. Berthod, C. W. Rischau, A. Ataei, L. Chen, S. Komiya, S. Ono, L. Taillefer, D. van der Marel, and A. Georges, Reconciling scaling of the optical conductivity of cuprate superconductors with Planckian resistivity and specific heat, Nat. Commun. **14**, 3033 (2023).

[9] A. Legros, S. Benhabib, W. Tabis, F. Laliberté, M. Dion, M. Lizaire, B. Vignolle, D. Vignolles, H. Raffy, Z. Z. Li, P. Auban-Senzier, N. Doiron-Leyraud, P. Fournier, D. Colson, L. Taillefer, and C. Proust, Universal T-linear resistivity and Planckian dissipation in overdoped cuprates, Nat. Phys. **15**, 142 (2019).

[10] S. Kasahara, T. Shibauchi, K. Hashimoto, K. Ikada, S. Tonegawa, R. Okazaki, H. Shishido, H. Ikeda, H. Takeya, K. Hirata, T. Terashima, and Y. Matsuda, Evolution from non-Fermi- to Fermi-liquid transport via isovalent doping in $BaFe_2(As_{1-x}P_x)_2$ superconductors, Phys. Rev. B **81**, 184519 (2010).

[11] E. Abrahams and Q. Si, Quantum criticality in the iron pnictides and chalcogenides, J. Phys. Condens. Matter **23**, 223201 (2011).

[12] A. Chubukov and P. J. Hirschfeld, Iron-based superconductors, seven years later, Phys. Today **68**, No. 6, 46 (2015).

[13] Q. Si and N. E. Hussey, Iron-based superconductors: Teenage, complex, challenging, Phys. Today **76**, No. 5, 34 (2023).

[14] J. G. Analytis, H.-H. Kuo, R. D. McDonald, M. Wartenbe, P. M. C. Rourke, N. E. Hussey, and I. R. Fisher, Transport near a quantum critical point in $BaFe_2(As_{1-x}P_x)_2$, Nat. Phys. **10**, 194 (2014).

[15] I. M. Hayes, R. D. McDonald, N. P. Breznay, T. Helm, P. J. W. Moll, M. Wartenbe, A. Shekhter, and J. G. Analytis, Scaling between magnetic field and temperature in the high-temperature superconductor $BaFe_2(As_{1-x}P_x)_2$, Nat. Phys. **12**, 916 (2016).

[16] W. K. Huang, S. Hosoi, M. Čulo, S. Kasahara, Y. Sato, K. Matsuura, Y. Mizukami, M. Berben, N. E. Hussey, H. Kontani, T. Shibauchi, and Y. Matsuda, Non-fermi liquid transport in the vicinity of the nematic quantum critical point of superconducting $FeSe_{1-x}S_x$, Phys. Rev. Res. **2**, 033367 (2020).

[17] X. Jiang, M. Qin, X. Wei, L. Xu, J. Ke, H. Zhu, R. Zhang, Z. Zhao, Q. Liang, Z. Wei, Z. Lin, Z. Feng, F. Chen, P. Xiong, J. Yuan, B. Zhu, Y. Li, C. Xi, Z. Wang, M. Yang, J. Wang, T. Xiang, J. Hu, K. Jiang, Q. Chen, K. Jin, and Z. Zhao, Interplay between superconductivity and the strange-metal state in FeSe, Nat. Phys. **19**, 365 (2023).

[18] Y. Cao, V. Fatemi, S. Fang, K. Watanabe, T. Taniguchi, E. Kaxiras, and P. Jarillo-Herrero, Unconventional superconductivity in magic-angle graphene superlattices, Nature (London) **556**, 43 (2018).

[19] Y. Cao, D. Chowdhury, D. Rodan-Legrain, O. Rubies-Bigorda, K. Watanabe, T. Taniguchi, T. Senthil, and P. Jarillo-Herrero, Strange metal in magic-angle graphene with near Planckian dissipation, Phys. Rev. Lett. **124**, 076801 (2020).

[20] A. Jaoui, I. Das, G. Di Battista, J. Díez-Mérida, X. Lu, K. Watanabe, T. Taniguchi, H. Ishizuka, L. Levitov, and D. K. Efetov, Quantum critical behaviour in magic-angle twisted bilayer graphene, Nat. Phys. **18**, 633 (2022).

[21] H. von Löhneysen, Non-Fermi-liquid behaviour in the heavy-fermion system $CeCu_{6-x}Au_x$, J. Phys. Condens. Matter **8**, 9689 (1996).

[22] O. Trovarelli, C. Geibel, S. Mederle, C. Langhammer, F. M. Grosche, P. Gegenwart, M. Lang, G. Sparn, and F. Steglich, $YbRh_2Si_2$: Pronounced non-Fermi-liquid effects above a low-lying magnetic phase transition, Phys. Rev. Lett. **85**, 626 (2000).

[23] J. Paglione, M. A. Tanatar, D. G. Hawthorn, E. Boaknin, R. W. Hill, F. Ronning, M. Sutherland, L. Taillefer, C. Petrovic, and P. C. Canfield, Field-induced quantum critical point in $CeCoIn_5$, Phys. Rev. Lett. **91**, 246405 (2003).

[24] L. Prochaska, X. Li, D. C. MacFarland, A. M. Andrews, M. Bonta, E. F. Bianco, S. Yazdi, W. Schrenk, H. Detz, A. Limbeck, Q. Si, E. Ringe, G. Strasser, J. Kono, and S. Paschen, Singular charge fluctuations at a magnetic quantum critical point, Science **367**, 285 (2020).

[25] M. Taupin and S. Paschen, Are heavy fermion strange metals Planckian?, Crystals **12**, 251 (2022).

[26] X. Li, J. Kono, Q. Si, and S. Paschen, Is the optical conductivity of heavy fermion strange metals Planckian?, Front. Electron. Mater. **2**, 934691 (2023).

[27] L. Chen, D. T. Lowder, E. Bakali, A. M. Andrews, W. Schrenk, M. Waas, R. Svagera, G. Eguchi, L. Prochaska, Y. Wang, C. Setty, S. Sur, Q. Si, S. Paschen, and D. Natelson, Shot noise in a strange metal, Science **382**, 907 (2023).

[28] D. H. Nguyen, A. Sidorenko, M. Taupin, G. Knebel, G. Lapertot, E. Schuberth, and S. Paschen, Superconductivity in an extreme strange metal, Nat. Commun. **12**, 4341 (2021).

[29] M. C. Aronson, R. Osborn, R. A. Robinson, J. W. Lynn, R. Chau, C. L. Seaman, and M. B. Maple, Non-Fermi-liquid scaling of the magnetic response in $UCu_{5-x}Pd_x (x = 1, 1.5)$, Phys. Rev. Lett. **75**, 725 (1995).

[30] A. Schröder, G. Aeppli, R. Coldea, M. Adams, O. Stockert, H. Löhneysen, E. Bucher, R. Ramazashvili, and P. Coleman, Onset of antiferromagnetism in heavy-fermion metals, Nature (London) **407**, 351 (2000).

[31] L. Poudel, J. M. Lawrence, L. S. Wu, G. Ehlers, Y. Qiu, A. F. May, F. Ronning, M. D. Lumsden, D. Mandrus, and A. D. Christianson, Multicomponent fluctuation spectrum at the quantum critical point in $CeCu_{6-x}Ag_x$, npj Quantum Mater. **4**, 52 (2019).

[32] C.-J. Yang, S. Pal, F. Zamani, K. Kliemt, C. Krellner, O. Stockert, H. v. Löhneysen, J. Kroha, and M. Fiebig, Terahertz conductivity of heavy-fermion systems from time-resolved spectroscopy, Phys. Rev. Res. **2**, 033296 (2020).

[33] G. Giuliani and G. Vignale, *Quantum Theory of the Electron Liquid* (Cambridge University Press, Cambridge, England, 2005), 10.1017/CBO9780511619915.

[34] D. V. Else, R. Thorngren, and T. Senthil, Non-Fermi liquids as ersatz Fermi liquids: General constraints on compressible metals, Phys. Rev. X **11**, 021005 (2021).

[35] D. V. Else and T. Senthil, Strange metals as ersatz Fermi liquids, Phys. Rev. Lett. **127**, 086601 (2021).

[36] C. M. Varma, P. B. Littlewood, S. Schmitt-Rink, E. Abrahams, and A. E. Ruckenstein, Phenomenology of the normal state of Cu-O high-temperature superconductors, Phys. Rev. Lett. **63**, 1996 (1989).

[37] A. A. Patel, H. Guo, I. Esterlis, and S. Sachdev, Universal theory of strange metals from spatially random interactions, Science **381**, 790 (2023).

[38] E. E. Aldape, T. Cookmeyer, A. A. Patel, and E. Altman, Solvable theory of a strange metal at the breakdown of a heavy Fermi liquid, Phys. Rev. B **105**, 235111 (2022).

[39] P. Cha, N. Wentzell, O. Parcollet, A. Georges, and E.-A. Kim, Linear resistivity and Sachdev-Ye-Kitaev (SYK) spin liquid behavior in a quantum critical metal with spin-$1/2$ fermions, Proc. Natl. Acad. Sci. U.S.A. **117**, 18341 (2020).

[40] A. Georges, G. Kotliar, W. Krauth, and M. J. Rozenberg, Dynamical mean-field theory of strongly correlated fermion systems and the limit of infinite dimensions, Rev. Mod. Phys. **68**, 13 (1996).

[41] T. A. Maier, M. Jarrell, T. Pruschke, and M. Hettler, Quantum cluster theories, Rev. Mod. Phys. **77**, 1027 (2005).

[42] F. Rullier-Albenque, P. A. Vieillefond, H. Alloul, A. W. Tyler, P. Lejay, and J. F. Marucco, Universal T_c depression by irradiation defects in underdoped and overdoped cuprates?, Europhys. Lett. **50**, 81 (2000).

[43] M. A. Tanatar, J. Paglione, C. Petrovic, and L. Taillefer, Anisotropic violation of the Wiedemann-Franz law at a quantum critical point, Science **316**, 1320 (2007).

[44] T. R. Chien, Z. Z. Wang, and N. P. Ong, Effect of Zn impurities on the normal-state Hall angle in single-crystal $YBa_2Cu_{3-x}Zn_xO_{7-\delta}$, Phys. Rev. Lett. **67**, 2088 (1991).

[45] A. Carrington, A. P. Mackenzie, C. T. Lin, and J. R. Cooper, Temperature dependence of the Hall angle in single-crystal $YBa_2(Cu_{1-x}Co_x)_3O_{7-\delta}$, Phys. Rev. Lett. **69**, 2855 (1992).

[46] S. Paschen, T. Lühmann, S. Wirth, P. Gegenwart, O. Trovarelli, C. Geibel, F. Steglich, P. Coleman, and Q. Si, Hall-effect evolution across a heavy-fermion quantum critical point, Nature (London) **432**, 881 (2004).

[47] Y. Nakajima, K. Izawa, Y. Matsuda, S. Uji, T. Terashima, H. Shishido, R. Settai, Y. Onuki, and H. Kontani, Normal-state Hall angle and magnetoresistance in quasi-2d heavy fermion $CeCoIn_5$ near a quantum critical point, J. Phys. Soc. Jpn. **73**, 5 (2004).

[48] Y. Nakajima, H. Shishido, H. Nakai, T. Shibauchi, K. Behnia, K. Izawa, M. Hedo, Y. Uwatoko, T. Matsumoto, R. Settai, Y. Ōnuki, H. Kontani, and Y. Matsuda, Non-Fermi liquid behavior in the magnetotransport of $CeMIn_5$ (M: Co and Rh): Striking similarity between quasi two-dimensional heavy fermion and high-T_c cuprates, J. Phys. Soc. Jpn. **76**, 024703 (2007).

[49] M. Čulo, M. Berben, Y.-T. Hsu, J. Ayres, R. D. H. Hinlopen, S. Kasahara, Y. Matsuda, T. Shibauchi, and N. E. Hussey, Putative Hall response of the strange metal component in $FeSe_{1-x}S_x$, Phys. Rev. Res. **3**, 023069 (2021).

[50] R. Lyu, Z. Tuchfeld, N. Verma, H. Tian, K. Watanabe, T. Taniguchi, C. N. Lau, M. Randeria, and M. Bockrath, Strange metal behavior of the Hall angle in twisted bilayer graphene, Phys. Rev. B **103**, 245424 (2021).

[51] Q. Si, S. Rabello, K. Ingersent, and J. L. Smith, Locally critical quantum phase transitions in strongly correlated metals, Nature (London) **413**, 804 (2001).

[52] P. Coleman, C. Pépin, Q. Si, and R. Ramazashvili, How do Fermi liquids get heavy and die?, J. Phys. Condens. Matter **13**, R723 (2001).

[53] P. Coleman and C. Pépin, What is the fate of the heavy electron at a quantum critical point?, Physica (Amsterdam) **312–313B**, 383 (2002).

[54] T. Senthil, S. Sachdev, and M. Vojta, Fractionalized Fermi liquids, Phys. Rev. Lett. **90**, 216403 (2003).

[55] T. Senthil, M. Vojta, and S. Sachdev, Weak magnetism and non-Fermi liquids near heavy-fermion critical points, Phys. Rev. B **69**, 035111 (2004).

[56] A. Gleis, S.-S. B. Lee, G. Kotliar, and J. von Delft, Emergent properties of the periodic Anderson model: A high-resolution, real-frequency study of heavy-fermion quantum criticality, Phys. Rev. X **14**, 041036 (2024).

[57] L. Zhu, S. Kirchner, Q. Si, and A. Georges, Quantum critical properties of the Bose-Fermi Kondo model in a large-N limit, Phys. Rev. Lett. **93**, 267201 (2004).

[58] M. T. Glossop, S. Kirchner, J. H. Pixley, and Q. Si, Critical Kondo destruction in a pseudogap Anderson model: Scaling and relaxational dynamics, Phys. Rev. Lett. **107**, 076404 (2011).

[59] A. Cai, Z. Yu, H. Hu, S. Kirchner, and Q. Si, Dynamical scaling of charge and spin responses at a Kondo destruction quantum critical point, Phys. Rev. Lett. **124**, 027205 (2020).

[60] Y. Komijani and P. Coleman, Emergent critical charge fluctuations at the Kondo breakdown of heavy fermions, Phys. Rev. Lett. **122**, 217001 (2019).

[61] P. Sun and G. Kotliar, Understanding the heavy fermion phenomenology from a microscopic model, Phys. Rev. Lett. **95**, 016402 (2005).

[62] D. Tanasković, K. Haule, G. Kotliar, and V. Dobrosavljević, Phase diagram, energy scales, and nonlocal correlations in the Anderson lattice model, Phys. Rev. B **84**, 115105 (2011).

[63] L. De Leo, M. Civelli, and G. Kotliar, Cellular dynamical mean-field theory of the periodic Anderson model, Phys. Rev. B **77**, 075107 (2008).

[64] L. De Leo, M. Civelli, and G. Kotliar, $T = 0$ heavy-fermion quantum critical point as an orbital-selective Mott transition, Phys. Rev. Lett. **101**, 256404 (2008).

[65] G. Kotliar, S. Y. Savrasov, G. Pálsson, and G. Biroli, Cellular dynamical mean field approach to strongly correlated systems, Phys. Rev. Lett. **87**, 186401 (2001).

[66] K. G. Wilson, The renormalization group: Critical phenomena and the Kondo problem, Rev. Mod. Phys. **47**, 773 (1975).

[67] R. Bulla, T. A. Costi, and T. Pruschke, Numerical renormalization group method for quantum impurity systems, Rev. Mod. Phys. **80**, 395 (2008).

[68] A. Weichselbaum and J. von Delft, Sum-rule conserving spectral functions from the numerical renormalization group, Phys. Rev. Lett. **99**, 076402 (2007).

[69] A. Weichselbaum, Tensor networks and the numerical renormalization group, Phys. Rev. B **86**, 245124 (2012).

[70] S.-S. B. Lee and A. Weichselbaum, Adaptive broadening to improve spectral resolution in the numerical renormalization group, Phys. Rev. B **94**, 235127 (2016).

[71] S.-S. B. Lee, J. von Delft, and A. Weichselbaum, Doublon-holon origin of the subpeaks at the Hubbard band edges, Phys. Rev. Lett. **119**, 236402 (2017).

[72] B. A. Jones, C. M. Varma, and J. W. Wilkins, Low-temperature properties of the two-impurity Kondo Hamiltonian, Phys. Rev. Lett. **61**, 125 (1988).

[73] B. A. Jones and C. M. Varma, Critical point in the solution of the two magnetic impurity problem, Phys. Rev. B **40**, 324 (1989).

[74] I. Affleck and A. W. W. Ludwig, Exact critical theory of the two-impurity Kondo model, Phys. Rev. Lett. **68**, 1046 (1992).

[75] I. Affleck, A. W. W. Ludwig, and B. A. Jones, Conformal-field-theory approach to the two-impurity Kondo problem: Comparison with numerical renormalization-group results, Phys. Rev. B **52**, 9528 (1995).

[76] B. A. Jones, Kondo effect, in *Handbook of Magnetism and Advanced Magnetic Materials*, edited by H. Kronmüller and S. Parkin (Wiley, New York, 2007), Vol. 1, 10.1002/9780470022184.hmm106.

[77] A. K. Mitchell and E. Sela, Universal low-temperature crossover in two-channel Kondo models, Phys. Rev. B **85**, 235127 (2012).

[78] A. K. Mitchell, E. Sela, and D. E. Logan, Two-channel Kondo physics in two-impurity Kondo models, Phys. Rev. Lett. **108**, 086405 (2012).

[79] O. Sakai, Y. Shimizu, and T. Kasuya, Excitation spectra of two impurity Anderson model, Solid State Commun. **75**, 81 (1990).

[80] O. Sakai and Y. Shimizu, Excitation spectra of the two impurity Anderson model. I. Critical transition in the two magnetic impurity problem and the roles of the parity splitting, J. Phys. Soc. Jpn. **61**, 2333 (1992).

[81] J. B. Silva, W. L. C. Lima, W. C. Oliveira, J. L. N. Mello, L. N. Oliveira, and J. W. Wilkins, Particle-hole asymmetry in the two-impurity Kondo model, Phys. Rev. Lett. **76**, 275 (1996).

[82] M. Fabrizio, A. F. Ho, L. D. Leo, and G. E. Santoro, Nontrivial fixed point in a twofold orbitally degenerate Anderson impurity model, Phys. Rev. Lett. **91**, 246402 (2003).

[83] L. D. Leo and M. Fabrizio, Spectral properties of a two-orbital Anderson impurity model across a non-Fermi-liquid fixed point, Phys. Rev. B **69**, 245114 (2004).

[84] R. M. Fye, anomalous fixed point behavior of two Kondo impurities: A reexamination, Phys. Rev. Lett. **72**, 916 (1994).

[85] A. Nejati, K. Ballmann, and J. Kroha, Kondo destruction in RKKY-coupled Kondo lattice and multi-impurity systems, Phys. Rev. Lett. **118**, 117204 (2017).

[86] B. Lechtenberg, F. Eickhoff, and F. B. Anders, Realistic quantum critical point in one-dimensional two-impurity models, Phys. Rev. B **96**, 041109(R) (2017).

[87] F. Eickhoff, B. Lechtenberg, and F. B. Anders, Effective low-energy description of the two-impurity Anderson model: RKKY interaction and quantum criticality, Phys. Rev. B **98**, 115103 (2018).

[88] F. Eickhoff and F. B. Anders, Strongly correlated multi-impurity models: The crossover from a single-impurity problem to lattice models, Phys. Rev. B **102**, 205132 (2020).

[89] See Supplemental Material at http://link.aps.org/supplemental/10.1103/PhysRevLett.134.106501 for additional information on the phase diagram and SYK dynamics, basic formulas involving the optical conductivity, the numerical computation of the optical conductivity, the role of vertex contributions, the Drude weight, the scaling functions, and scaling of the complex optical conductivity and an estimate of the suitability of our model parameters for the description of $CeCoIn_5$, which includes Refs. [90–101].

[90] P. Nozières, A “Fermi-liquid” description of the Kondo problem at low temperatures, J. Low Temp. Phys. **17**, 31 (1974).

[91] R. Resta, Drude weight and superconducting weight, J. Phys. Condens. Matter **30**, 414001 (2018).

[92] D. J. Scalapino, S. R. White, and S. Zhang, Insulator, metal, or superconductor: The criteria, Phys. Rev. B **47**, 7995 (1993).

[93] A. K. Mitchell, M. R. Galpin, S. Wilson-Fletcher, D. E. Logan, and R. Bulla, Generalized Wilson chain for solving multichannel quantum impurity problems, Phys. Rev. B **89**, 121105(R) (2014).

[94] K. M. Stadler, A. K. Mitchell, J. von Delft, and A. Weichselbaum, Interleaved numerical renormalization group as an efficient multiband impurity solver, Phys. Rev. B **93**, 235101 (2016).

[95] F. B. Kugler, Improved estimator for numerical renormalization group calculations of the self-energy, Phys. Rev. B **105**, 245132 (2022).

[96] Because of singular features developing in the self-consistent hybridization function close to the QCP [56], it is numerically not possible to tune exactly to the QCP.

[97] A. Weichselbaum, Non-Abelian symmetries in tensor networks: A quantum symmetry space approach, Ann. Phys. (N.Y.) **327**, 2972 (2012).

[98] A. Weichselbaum, X-symbols for non-Abelian symmetries in tensor networks, Phys. Rev. Res. **2**, 023385 (2020).

[99] A. Weichselbaum, QSpace—an open source tensor library for Abelian and non-Abelian symmetries, SciPost Phys. Codebases 40 (2024).

[100] We call frequency dependences $(\omega^a - 1)/a$ with $a \simeq 0$ logarithmic if the exponent a cannot be reasonably distinguished from $a \to 0$ based on our numerical data. Ditto for temperature dependences. Similarly, “plateau” means ω^a with $a \simeq 0$ and “linear” ω^a with $a \simeq 1$.

[101] S.-S. B. Lee, F. B. Kugler, and J. von Delft, Computing local multipoint correlators using the numerical renormalization group, Phys. Rev. X **11**, 041007 (2021).

[102] F. B. Kugler, S.-S. B. Lee, and J. von Delft, Multipoint correlation functions: Spectral representation and numerical evaluation, Phys. Rev. X **11**, 041006 (2021).

[103] J.-M. Lihm, J. Halbinger, J. Shim, J. von Delft, F. B. Kugler, and S.-S. B. Lee, Symmetric improved estimators for multipoint vertex functions, Phys. Rev. B **109**, 125138 (2024).

[104] In the PAM, $\mathbf{G}_{\mathbf{k}}(\omega)$ is matrix valued in the orbital space, with orbital index $\alpha \in \{f, c\}$. $G^{-1}_{\mathbf{k}_\mathrm{F}}(\omega)$ is defined in terms of the eigenvalue which fulfills $\mathrm{Re}G^{-1}_{\mathbf{k}_\mathrm{F}}(0) = 0$. To determine the single-particle decay rate γ^*, the ω dependence of the corresponding eigenvalue is fitted to a Lorentzian line shape around $\omega = 0$, $G_{\mathbf{k}_\mathrm{F}}(\omega) \simeq Z/(\omega + \mathrm{i}\gamma^*)$, as usual.

[105] P. Coleman, *Introduction to Many-Body Physics* (Cambridge University Press, Cambridge, England, 2015).

[106] L. Y. Shi, Z. Tagay, J. Liang, K. Duong, Y. Wu, F. Ronning, D. G. Schlom, K. Shen, and N. P. Armitage, Low energy electrodynamics and a hidden Fermi liquid in the heavy-fermion $CeCoIn_5$, arXiv:2310.10916.